

1 **Regional and seasonal variations of the Twomey indirect effect as observed by**
2 **the ATSR-2 satellite instrument**

3
4 Claire E. Bulgin, Paul I. Palmer
5 School of Geosciences, University of Edinburgh, UK

6
7 Gareth E. Thomas, Christopher P.G. Arnold, Elies Campmany, Elisa Carboni, Roy G.
8 Grainger
9 Atmospheric, Oceanic and Planetary Physics, University of Oxford, UK

10
11 Caroline Poulsen, Richard Siddans, Bryan N. Lawrence
12 Rutherford Appleton Laboratory, Oxfordshire, UK

13
14 **Abstract**

15 We use satellite observations of aerosol optical depth τ_a and cloud effective radius r_e
16 from the ATSR-2 instrument in 1997 to investigate the Twomey indirect effect (IE, -
17 $\partial \ln r_e / \partial \ln \tau_a$) in regions of continental outflow. We generally find a negative
18 correlation between τ_a and r_e , with the strongest inverse relationships downwind of
19 Africa. North American and eastern Asian continental outflow exhibits a strong
20 seasonal dependence, as expected. Global values for IE range from 0.10 to 0.16,
21 consistent with theoretical predictions. Downwind of Africa, we find that the IE is
22 unphysically high but robust ($r=-0.85$) during JJA associated with high aerosol
23 loading, and attribute this tentatively to the Twomey hypothesis accounting only for a
24 limited number of physical properties of aerosols.

25
26 **Introduction**

27 Atmospheric aerosols represent one of the largest uncertainties in current
28 understanding of Earth's climate [IPCC, 2007]. Aerosols affect the atmospheric
29 radiation balance by absorbing and scattering solar radiation (direct effect), the
30 magnitude of such effects depends on a number of factors including chemical
31 composition, size distribution, and mixing state. Aerosols also affect cloud radiative

32 properties by acting as cloud condensation nuclei, CCN (indirect effects, IE),
33 depending on size and chemical composition. Assuming constant liquid water content
34 (LWC), elevated concentrations of aerosols increase the cloud droplet number and
35 subsequently reduce the mean cloud droplet size, leading to an increase in cloud
36 albedo [Twomey, 1974]. Reduced cloud droplet size suppresses precipitation and
37 increases cloud lifetime [Albrecht, 1989]. Accurate modelling of these indirect effects
38 involves detailed aerosol microphysics, and is therefore difficult to use in large-scale
39 chemistry-climate models [IPCC, 2007].

40

41 There are a number of anthropogenic and natural sources of aerosols [Seinfeld and
42 Pandis, 1998]. The main sinks of aerosols are gravitational settling and wet
43 deposition, the relative importance of these depends on the aerosol physical and
44 chemical properties, leading to lifetimes of typically a few days. Such short lifetimes
45 lead to rapid spatial and temporal variations in loading and chemical composition that
46 are not well suited for study by sparse ground-based measurement networks. Satellite
47 observations offer a global perspective but currently they only measure a small
48 number of aerosol and cloud optical properties, e.g. optical depth and single scattering
49 albedo [IPCC, 2007]. A number of previous studies using data from satellite sensors
50 show an inverse correlation between aerosol optical depths (used as a proxy for
51 aerosol number) and cloud droplet properties in continental outflow (e.g., Avey et al,
52 [2007]) or globally (e.g., Breon et al, [2002]).

53

54 Here, we use satellite observations of aerosol and cloud optical properties from the
55 Global Retrieval of ATSR Cloud Parameter and Evaluation (GRAPE) dataset [Watts
56 et al. 2000; Marsh et al. 2004], to quantify the Twomey IE, as discussed below. In this

57 analysis we use cloud droplet effective radius, r_e , the area weighted mean radius of
58 cloud droplets, and aerosol optical depth, τ_a , a measure of total column light
59 extinction due to scattering and absorption of aerosol particles.

60

61 **Data**

62 The second Along-Track Scanning Radiometer (ATSR-2), aboard the ERS-2 satellite,
63 observes reflected solar radiation in the visible and infrared using seven spectral
64 channels. ERS-2 is in a near-polar, sun-synchronous orbit with an equator overpass
65 time of 10:30 in the descending node. ATSR-2 has a 512km swath width in the nadir,
66 achieving global coverage every three days.

67

68 Aerosol and cloud properties are derived using the Oxford/RAL Aerosol and Cloud
69 (ORAC) optimal estimation retrieval scheme that was developed for clouds [Watts et
70 al., 1998] and extended to aerosols [Marsh et al., 2004]. The retrieval scheme
71 averages a block of 12 ATSR-2 pixels to achieve an effective resolution of 2.6km
72 across-track and 3.5km along-track. The scheme uses the Discrete Ordinates
73 Radiative Transfer model [Stammes et al., 1988] to calculate the top of atmosphere
74 radiance as a function of the properties of a plane parallel cloud layer or aerosol with
75 an assumed height distribution. ORAC fits the radiance in all channels by varying all
76 retrieved parameters simultaneously, while accounting for *a priori* information. The
77 scheme also provides error estimates on all retrieved quantities.

78

79 Cloud flagging is performed prior to retrieval. Over the ocean the difference between
80 the observed thermal radiance and a clear sky value predicted by radiative transfer
81 calculations is used. We also employ an additional test to detect low, warm clouds

82 over the ocean and clouds over land based on surface reflectance at 0.67 and 0.87 μm
83 [Birks, 2007]. Cloud properties are retrieved using the 0.67, 0.87, 1.6, 11 and 12 μm
84 channels and the derived products are optical depth at 0.55 μm , effective radius, LWP,
85 cloud top height, pressure and temperature and cloud fraction. Aerosol optical depth
86 at 0.55 μm and aerosol effective radius are retrieved using the 0.67, 0.87 and 1.6 μm
87 channels. The Optical Properties of Aerosol and Clouds (OPAC) inventory provides
88 the *a priori* information on aerosol optical properties [Hess et al. 1998], with the
89 aerosol type used in each pixel being assigned from aerosol climatology.

90

91 Validation of both cloud and aerosol properties derived using the GRAPE algorithm is
92 ongoing [Poulsen and Watts, 2002; Kokhanovsky et al., 2007; Thomas et al., 2007].
93 We use only retrieved aerosol and cloud data where the retrieval algorithm converged
94 within 10 iterations. For cloud data we use retrievals that have cloud top heights
95 below 3km (with an error of <200m), ensuring that we use only low-level clouds that
96 are most likely to be influenced by boundary layer outflow [Keil and
97 Haywood, 2003]. Measurements of r_e below 2 μm are removed to prevent
98 contamination of cloud retrievals with erroneously flagged aerosol; r_e values above 25
99 μm , representing <10% of data, are unrealistic for low-level cloud and have also been
100 filtered from the data. We only consider aerosol retrievals that have τ_a errors < 0.25.

101

102 **Results**

103 Figure 1 shows monthly mean values of τ_a and r_e in January and July 1997 averaged
104 on a regular 1°x1° grid. Observed τ_a values are typically 0-0.8 with the highest values
105 reaching 2 over the eastern Atlantic downwind of Africa. During January there are
106 elevated values of τ_a over the western Pacific, the Arabian Sea, the Bay of Bengal, the

107 South China Sea, the eastern tropical Atlantic, and the Southern Ocean. There are
108 similar distributions of elevated τ_a during July but with smaller values over the
109 western Pacific and higher values over the midlatitude western Atlantic downwind of
110 North America. Values of r_e range from 5 to 25 μm with the smallest values observed
111 over the oceans in regions of continental outflow.

112

113 We quantify the Twomey IE over four regions of continental outflow, ensuring a fresh
114 supply of aerosols for cloud droplet formation: eastern equatorial Atlantic (North
115 Africa), eastern South Atlantic (Southern Africa), western mid-latitude North Atlantic
116 (North America), and western North Pacific (eastern Asia). We also consider data
117 over the remote Pacific (used as a control), and over the globe. Table 1 defines the
118 geographical regions shown in Figure 1. We find the largest τ_a values over the eastern
119 South Atlantic, downwind of Africa (Figure 1). The southward migration of elevated
120 τ_a over that region during 1997 (not shown) reflects the burning season in Africa, and
121 is consistent with the spatial distribution of ATSR firecounts. In DJF analysis for the
122 eastern South Atlantic is in a box just below the Saharan region (Figure 1) in order to
123 capture this seasonal variation in biomass burning.

124

125 Previous studies have argued that aerosol index (AI), a measure of the wavelength
126 dependence of aerosol extinction, is a better quantity to test the Twomey hypothesis
127 because it is sensitive to the fine fraction of aerosol that is more likely to serve as
128 CCN [Breon et al. 2002; Quaas et al. 2004]. AI is not directly retrieved in the GRAPE
129 algorithm but can be approximated by the product of τ_a and the Angström exponent
130 (A). The Angström exponent varies inversely with particle size, the difference
131 between extinction coefficients being greater with smaller particles as determined by

132 Mie scattering. We approximate A using $A \approx \log(b_{ext1}/b_{ext2})/\log(\lambda_1/\lambda_2)$, where λ
133 represents wavelength and b_{ext} represents an extinction coefficient related to a
134 particular aerosol class and effective radius [Seinfeld and Pandis, 1998]. Here, we
135 evaluate A at 0.55 and 0.67 μm , where b_{ext} is defined as a function of aerosol effective
136 radius. OPAC classifications give values of b_{ext} according to wavelength, dependent
137 on the mixing ratio of each aerosol component in the aerosol class [Hess et al. 1998].
138 This mixing ratio is then varied in order to calculate b_{ext} as a function of aerosol
139 effective radius [Thomas et al. 2007].

140

141 A major criticism of using satellite data to test relationships between aerosol and
142 cloud properties has been that these properties are not measured coincidentally [Avey
143 et al. 2007]. Previous studies have used back-trajectories to link cloud and aerosol
144 properties (e.g. Breon et al. 2002), or colocated cloud retrievals and trace gas
145 measurements using a tracer transport model [Avey et al. 2007]. Breon et al, [2002]
146 used back-trajectories to couple aerosol and cloud retrievals and found that the
147 distance between measurements is typically less than 100km. We argue here that
148 analysis of aerosol and cloud properties derived from multi-day and seasonal means
149 averaged at $1 \times 1^\circ$ resolution (approximately $100 \times 100 \text{km}^2$ at low and mid-latitudes)
150 negates the need to couple individual measurements.

151

152 Figure 2 shows a time series of τ_a , AI and r_e from 1st December 1996 to 31st January
153 1998, averaged individually across the six regions defined in Table 1. Standard
154 deviations for daily mean τ_a (AI) range from 0.04 to 0.06 (0.01-0.05), but can reach
155 up to 0.2 for τ_a and AI in strong continental outflow. Standard deviations for r_e
156 typically range from 4 to 6 μm . The 28-day rolling mean reduces the random noise on

157 the daily means. All regions that include continental outflow show coherent variations
158 in aerosol and cloud properties. The timing of the maximum values of τ_a and AI are
159 consistent with prior knowledge of outflow patterns, e.g. outflow over the western
160 Atlantic is at a maximum between June and August [Quinn and Bates, 2003]. There
161 is little variation in τ_a or AI over the remote Pacific, with values much less than those
162 observed in continental outflow, as expected.

163

164 The differences between τ_a and AI provide an indication of whether aerosols are
165 present mainly in the coarse ($>1\mu\text{m}$) or fine ($<1\mu\text{m}$) mode, as explained above. Figure
166 2 shows that τ_a is elevated above AI over the western Pacific in late spring when there
167 is strong outflow from the Asian continent that typically includes mineral dust
168 transport events [NCEP, 2007; Sang-Woo et al, 2006]. A similar discrepancy between
169 τ_a and AI occurs over the equatorial Atlantic downwind of the Sahara throughout the
170 year but is most pronounced between February and April, consistent with AI
171 retrievals from the Total Ozone Mapping Spectrometer. In contrast, North American
172 outflow over the Atlantic shows similar values for τ_a and AI, suggesting that fine
173 aerosols dominate that outflow. Variation of r_e depends on region. The smallest
174 values occur over the eastern Atlantic where we see large increases in τ_a . In general,
175 regions that include continental outflow show a negative relationship between τ_a or AI
176 and r_e , consistent with the Twomey IE. The region downwind of southern Africa
177 shows the strongest anti-correlation between AI and r_e ($r=-0.64$). For other regions the
178 correlation between τ_a or AI and r_e over 1997 is much weaker (Table 1), partly due to
179 the seasonal nature of continental outflow from many regions.

180

181 Similar anti-correlations could be generated from systematic sampling errors.
182 Erroneous cloud flagging, identifying high aerosol loading as cloudy pixels, would
183 result in very low values of r_e with elevated τ_a . It is likely that such a situation would
184 be identified by a bi-modal distribution in r_e measurements, which is not observed in
185 the GRAPE data. Aerosol and cloud layers may be decoupled across a frontal system
186 or if the atmosphere is vertically stable [Sinha et al. 2003] and in such situations anti-
187 correlations between τ_a and r_e do not signal a causal relationship. However, coastal
188 regions, typified by low-level cloud, experience cycling between stratiform and
189 cumuliform cloud layers [Paluch and Lenschow, 1991] so we expect aerosol and
190 cloud properties to be related over the spatial scales studied.

191

192 The Twomey IE can be described as the relative change in r_e associated with a
193 relative change in τ_a [Feingold et al. 2001]: $-\partial \ln r_e / \partial \ln \tau_a$. Assuming a homogeneous
194 cloud with a constant LWP, the relationship between cloud droplet number (N_d) and
195 the aerosol number concentration (N_a) is nonlinear: $N_d \propto N_a^\alpha$, where α is a unitless
196 parameter that provides an indication of particle hygroscopicity, with low values
197 corresponding to low hygroscopicity. A characteristic α value adopted by several
198 previous studies is 0.7 [Breon et al. 2002; Feingold et al. 2003]; below, we look at the
199 sensitivity of α to the interpretation of our results. As previously discussed, AI may
200 provide a better proxy for N_a [Breon et al. 2002; Quaas et al. 2004], but our analysis
201 concentrates on τ_a because AI is not a GRAPE retrieval product. It can be shown that
202 $r_e \propto \tau_a^{-\alpha/3}$ [Feingold, 2003] so using $\alpha=0.7$ gives $IE=\alpha/3 \approx 0.23$.

203

204 Table 1 shows the monthly mean values of IE and the associated correlation (r)
205 between τ_a and r_e for the defined regions. The gradients are calculated for τ_a between
206 0.13 and 0.4 with r_e averaged over τ_a increments of 0.03, accounting for the standard
207 error of the measurements in each size bin. Values of $\tau_a > 0.4$ are noisy, due to few
208 observations above this threshold, with the exception of southern African where
209 aerosol loading during the burning season is much greater than in other regions;
210 consequently we calculate IE for between 0.35 and 1.5 for DJF and JJA.

211

212 A physical condition of the assumed relationship between N_d and N_a is $\alpha \leq 1$ so that
213 $0 \leq IE \leq 0.33$. On a global scale, GRAPE data yields seasonal mean IE values
214 between 0.10 and 0.16 corresponding to values of α ranging from 0.30 to 0.48. The
215 theoretical value of $IE=0.23$ (assuming $\alpha=0.7$) is based only on the physical
216 relationship between aerosol number and cloud droplet number, disregarding other
217 important physical processes including aerosol size distribution and updraft velocity
218 [Feingold et al. 2001]. Previous studies have shown a similar range of IE values when
219 using this assumption (e.g. Feingold et al. 2003).

220

221 In the western North Atlantic, IE is strongest in JJA when continental outflow is
222 greatest. Over the western North Pacific the strongest IE is not observed during the
223 period of maximum outflow (MAM) when mineral dust is prevalent [Sang-Woo et al,
224 2006] but during DJF/SON when dust does not dominate the outflow. Over the
225 eastern South Atlantic we find significant IE values for DJF, JJA, and SON; there is
226 only a small amount of active burning during MAM (ESA, 2007). During JJA, we
227 find the IE is 0.51, implying an unphysical value of $\alpha > 1$. The high correlation
228 coefficient (-0.85) associated with this season suggests that the observed relationship

229 is not due to noisy data. In regions of high aerosol loading using the
230 assumption $N_d \approx N_a^\alpha$ may be an oversimplification. Feedback mechanisms associated
231 with drizzle suppression at the base of the cloud result in increased air entrainment
232 from above the cloud. Aerosol entrainment and activation may be enhanced
233 depending on the humidity of air above the cloud and the consequent effect on the
234 LWP [Ackerman et al. 2004]. During DJF we use the equatorial region to study
235 African burning outflow as noted above. Significant *IE* is found both here and in the
236 adjacent outflow region downwind of the Sahara desert, and we conclude that is
237 difficult to separate dust and burning outflow in this region although burning is more
238 likely responsible for the *IE* in this season. A weak *IE* is seen in the adjacent Saharan
239 region during JJA.

240

241 There are of course limitations to the theory outlined by Twomey [1974] and the
242 analysis approach we adopt in this paper, which we outline below. Recent work has
243 highlighted that the Twomey theory describes only the physical relationship between
244 aerosol number and cloud microphysics [Feingold et al. 2001, 2003]. Other physical
245 effects are not taken into account, most notably aerosol size distribution, which is
246 estimated to describe ~80% of the variability in aerosol activation [Duesk et al. 2006].
247 Although thought to take a secondary role, aerosol chemical composition is also
248 important in determining α and hence *IE* [Duesk et al. 2006]. Aerosols must be
249 hygroscopic in order to act as CCN; hydrophobic aerosol types such as desert dust
250 need to obtain a hydrophilic coating (e.g. sulphur or organics). Smaller aerosols from
251 industrial sources and biomass burning that contain organic species tend to be
252 hygroscopic and more immediately effective as CCN [Seinfeld and Pandis, 1998].

253

254 The Twomey hypothesis is based on the assumption that the cloud layer has a
255 homogenous LWC. Over the spatial scales measured by the satellite these
256 assumptions are unlikely to be valid: cycling between stratus layers and cumuli
257 clouds will lead to inhomogeneity [Paluch and Lenschow, 1991]. Air circulation
258 within the cloud, possibly modified by aerosol feedback mechanisms, will also result
259 in changing LWC [Ackerman et al. 2004]. The uncertainties in the derived IE values
260 in Table 1 are likely be underestimated because we do not account for variations in
261 LWC over the spatial scales studied. Despite the many assumptions we have made
262 our results are quantitatively consistent with theory at a global scale, and regionally
263 consistent during periods of high continental outflow.

264

265 **Acknowledgements**

266 CEB is supported by NERC DARC studentship NER/S/D/2006/14345, and via
267 additional support from the Rutherford Appleton Laboratory. The Oxford authors
268 wish to acknowledge NERC funding NER/T/S/2001/00205 and NE/B503933/1.

269

270 **References**

271

- 272 Ackerman A S, et al (2004). "The Impact of Humidity above Stratiform Clouds on
273 Indirect Aerosol Climate Forcing." Nature **432**:1014-1017.
- 274 Albrecht B A (1989). "Aerosols, Cloud Microphysics, and Fractional Cloudiness."
275 Science **245**(4923): 1227-1230.
- 276 Avey L, et al (2007). "Evaluation of the Aerosol Indirect Effect using Satellite, Tracer
277 Transport Model, and Aircraft Data from the International Consortium for
278 Atmospheric Research on Transport and Transformation." J. Geophys. Res. **112**.
- 279 Birks A (2007). "Improvements to the AATSR IPF relating to Land Surface
280 Temperature." ESA Technical Note.
- 281 Breon F M, et al (2002). "Aerosol Effect on Cloud Droplet Size Monitored from
282 Satellite." Science **295**: 834-838.
- 283 Duesk U, et al (2006). "Size Matters More Than Chemistry for Cloud-Nucleating
284 Ability of Aerosol Particles." Science **312**:1375-1378.
- 285 ESA (2007). "World Fire Atlas"
- 286 Feingold G, et al (2003). "First Measurements of the Twomey Indirect Effect using
287 Ground-Based Remote Sensors." Geophys. Res. Lett. **30**(6).

288 Feingold G, et al (2001). "Analysis of Smoke Impact on Clouds in Brazilian Biomass
289 Burning Regions: An Extension of Twomey's Approach." J. of Geophys. Res.
290 **106**(D19): 22,907-22,922.

291 Hess M, et al (1998). "Optical Properties of Aerosols and Clouds: The Software
292 Package OPAC." Bull. Am. Met. Soc. **79**(5): 831-844.

293 IPCC (2007). "Working Group 1: The Physical Basis of Climate Change." Working
294 Group 1 Fourth Assessment Report.

295 Keil A, Haywood J M. (2003). "Solar Radiative Forcing by Biomass Burning Aerosol
296 Particles during SAFARI 2000: A Case Study based on Measured Aerosol and
297 Cloud Properties." J. Geophys. Res. **108**(D13).

298 Kokhanovsky A A, et al (2007). "Aerosol Remote Sensing over Land: A Comparison
299 of Satellite Retrievals using Different Algorithms and Instruments." Atmospheric
300 Res.

301 Liu H, et al (2003). "Transport Pathways for Asian Pollution Outflow over the Pacific:
302 Interannual and Seasonal Variations." J. Geophys. Res. **108**(D20).

303 Marsh S H, et al (2004). "An Optimal Estimation Aerosol Retrieval Scheme for
304 ATSR-2." Atmospheric, Oceanic and Planetary Physics, Department of Physics,
305 University of Oxford

306 NCEP, National Oceanic and Atmospheric Administration (2007). "Earth System
307 Research Laboratory Physical Sciences Division: NCEP Reanalysis Electronic
308 Atlas.

309 Paluch I R, Lenschow D H (1991). "Stratiform Cloud Formation in the Marine
310 Boundary Layer." J. Atmos. Sci. **48**(19): 2141-2158.

311 Poulsen C, Watts P. (2002). "Retrieval and Validation of Cloud Properties using
312 ATSR-2 Data." EUMETSAT Meteorological Satellite Conference.

313 Quaas J, et al (2004). "Aerosol Indirect Effects in POLDER Satellite Data and the
314 Laboratoire de Meteorologie Dynamique-Zoom (LMDZ) General Circulation
315 Model." J. Geophys. Res. **109** (D08205).

316 Quinn P K, Bates T S. (2003). "North American, Asian, and Indian Haze: Similar
317 Regional Impacts on Climate?" Geophys. Res. Lett. **30**(11).

318 Sang-Woo K, Soon-Chang Y, Jiyoung K, Seung-Yeon K. (2006). "Seasonal and
319 Monthly Variations of Columnar Aerosol Optical Properties over east Asia
320 determined from multi-year MODIS, LIDAR, and AERONET Sun/Sky
321 Radiometer Measurements." Atmos. Env. **41**(8), 1634.

322 Seinfeld J H, Pandis S N. (1998). Atmospheric Chemistry and Physics: From Air
323 Pollution to Climate Change. United States of America, John Wiley & Sons, Inc.

324 Sinha P, Hobbs P V, Yokelson R J, Blake D R, Gao S, Kirchstetter T W. (2003).
325 "Distributions of Trace Gases and Aerosols During the Dry Biomass Burning
326 Season in Southern Africa." J. of Geophys. Res. **108**(D17).

327 Stammes K, et al (1988). "A Numerically Stable Algorithm for Discrete-Ordinate-
328 Method Radiative Transfer in Multiple Scattering and Emitting Layered Media.:
329 Appl. Opt. **27**:2502-2509.

330 Thomas G E, et al (2007). "Comparison of AATSR and SEVIRI Aerosol Retrievals
331 over the Northern Adriatic." Q. J. R. Met. Soc.

332 Thomas G E, et al (2007). "An Optimal Estimation Aerosol Retrieval Scheme for
333 (A)ATSR." Rutherford Appleton Laboratory.

334 Twomey, S. (1974). "Pollution and the Planetary Albedo." Atmos. Env. **8**: 1251-1256.

335 Watts P D, et al (1998). "Study on Cloud Properties derived from Meteosat Second
336 Generation Observations " EUMETSAT Report no 97/181.

337 Watts P D, et al (2000). "Aerosol Properties Derived from Meteosat Second
338 Generation." EUMETSAT Report.

339

340

341

342 Figure 1: Monthly mean τ_a (unitless) at $0.55 \mu\text{m}$ and r_e (μm) observed by ATSR-2
343 onboard ERS-2 during January and July 1997. Data are averaged on a regular $1^\circ \times 1^\circ$
344 grid with cloud data filtered for cloud top heights $<3\text{km}$, with an error associated with
345 this measure $<200\text{m}$, and for $2 \mu\text{m} < r_e < 25\mu\text{m}$. Aerosol data are filtered according to
346 τ_a error <0.25 . The striped structure in the plots is an artefact of ATSR-2 sampling.
347 The boxes indicate the regions defined in Table 1.

348

349 Figure 2: 28-day rolling mean of τ_a at $0.55 \mu\text{m}$ (light grey) and r_e (μm , black)
350 observed by ATSR-2 between 1st December 1996 and 31st January 1998 over the
351 globe, eastern South Atlantic, eastern equatorial Atlantic, western North Pacific,
352 western North Atlantic and the South Pacific. AI (dark grey) is calculated using
353 offline extinction coefficients at $0.55\mu\text{m}$ and $0.67\mu\text{m}$. Standard errors (standard
354 deviation/ $\sqrt{(n-2)}$) are superimposed on the time series but are close to zero.
355 Correlation coefficients between τ_a/AI (light grey/dark grey) and r_e are given in each
356 panel.

357 Table 1: Seasonal mean Twomey IE ($-\partial \ln r_e / \partial \ln \tau_a$) and associated correlations between r_e and τ_a during 1997.

358

Month	Globe ^a		Eastern S. Atlantic ^b (Africa)		Western N. Pacific ^c (Asia)		Western N. Atlantic ^d (North America)		Eastern Eq. Atlantic ^e (Sahara)		S. Pacific ^f	
	IE ^g	<i>r</i>	IE	<i>r</i>	IE	<i>r</i>	IE	<i>r</i>	IE	<i>r</i>	IE	<i>r</i>
DJF	0.13+/- 0.01 ^g	-0.75	0.20+/- 0.13 ^{k,l}	-0.36	0.12+/- 0.05	-0.68	-0.56+/- 0.13	0.92	0.10+/- 0.02	-0.88	-0.37+/- 0.08	0.36 ^h
MAM	0.13+/- 0.007	-0.87	-0.48+/- 0.03	0.38	-0.14+/- 0.01	0.56	0.11+/- 0.11 ^j	-0.44	-0.06+/- 0.03	0.74	0.001+/- 0.09 ^j	0.36 ^h
JJA	0.16+/- 0.01	-0.99	0.51+/- 0.16 ^{i,k}	-0.85	-0.04+/- 0.05 ^j	-0.13	0.16+/- 0.08	-0.78	0.16+/- 0.04	-0.48	-0.16+/- 0.09	0.36 ^h
SON	0.10+/- 0.01	-0.98	0.27+/- 0.05	-0.85	0.23+/- 0.06	-0.94	-0.16+/- 0.19 ^j	0.70	-0.03+/- 0.03 ^j	0.64	-0.37+/- 0.07	0.36 ^h

a: Region defined: 180W-180E, 45S-60N; τ_a : r_e correlation = 0.38; AI: r_e correlation = 0.68.

372 lation = 0.38; AI: r_e correlation=0.68.

373 b: Region defined: 10W–10E, 15S–5N; τ_a : r_e correlation = -0.39; AI: r_e correlation=-0.64.

374 c: Region defined: 140E–170E, 35N–45N; τ_a : r_e correlation = -0.47; AI: r_e correlation=-0.36.

375 d: Region defined: 60W–74W, 35N–43N; τ_a : r_e correlation = 0.23 AI: r_e correlation=0.37.

376 e: Region defined: 50W–15W, 15N–40N; τ_a : r_e correlation = -0.33; AI: r_e correlation=0.13.

377 f: Region defined: 120W–140W, 0N–20N; τ_a : r_e correlation = -0.17; AI: r_e correlation=0.16.

378 g: To obtain the gradient, r_e was averaged over τ_a size bins of 0.03, between 0.13 and 0.4 in the given region over the period of each season.

379 h: Shaded boxes represent an IE consistent with theory assuming $\alpha < 1$.

380 i: Regions where $N_d \approx (N_a)^\alpha$ cannot be assumed.

381 j: Regions where the retrieved IE value is not significant.

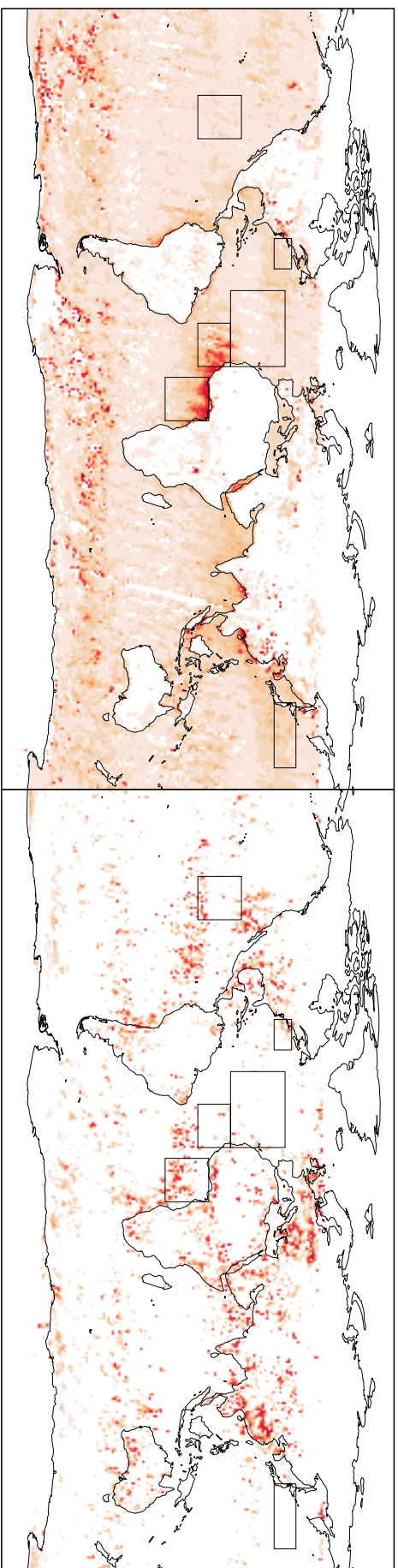
382 k: The gradient IE was calculated for τ_a values of 0.35–1.5.

383 l: Region defined: 15W–35W, 0N–15N.

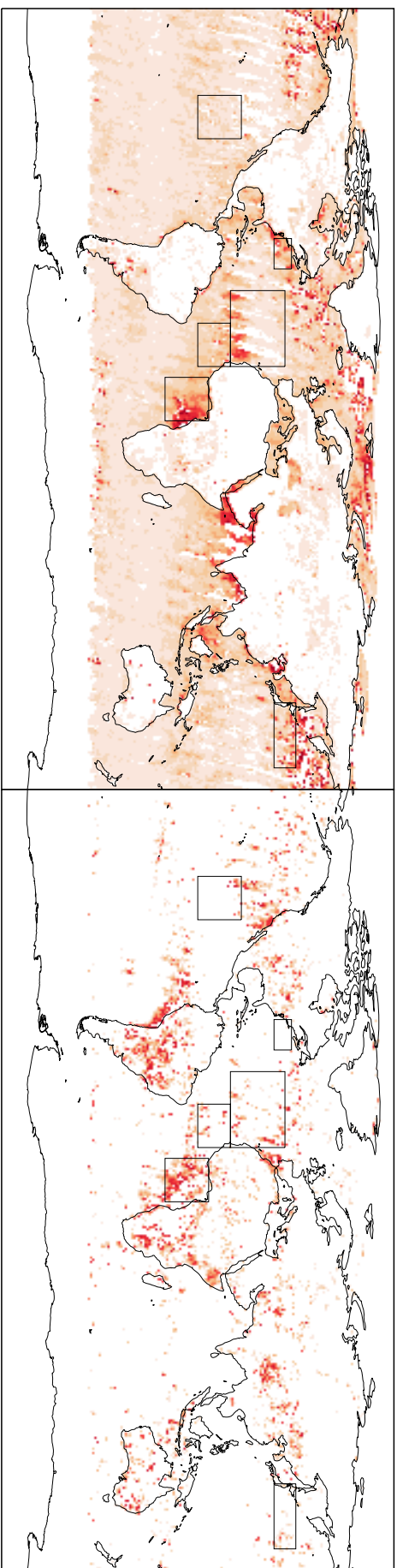
Aerosol Optical Depth

Cloud Effective Radius

JAN



JUL



< 0.00 2.00 > [unitless]

< 5 8 14 25 > [microns]

.33
 $r = 0.13$

